Journal of Computational and Applied Mathematics 281 (2015) 58–73

Contents lists available at ScienceDirect

Journal of Computational and Applied Mathematics

journal homepage: www.elsevier.com/locate/cam

Applying the combined integral method to two-phase Stefan problems with delayed onset of phase change

S.L. Mitchell

MACSI, Department of Mathematics and Statistics, University of Limerick, Limerick, Ireland

ARTICLE INFO

Article history:
Received 27 March 2014
Received in revised form 15 October 2014

Keywords:
Stefan problem
Two-phase
Heat balance integral method
Phase change

ABSTRACT

In this paper the combined integral method (CIM) is applied to non-classical two-phase Stefan problems with delayed onset of phase change. This can occur if the phase change is caused by a heat-flux or Robin boundary condition. The method requires choosing an approximating function, typically a polynomial, but it is not clear what should be used as the exponent in the highest order term. Previous studies have determined exponents either from exact solutions or from expansions valid over short time scales; neither approach is satisfactory and can be very inaccurate for larger times. We combined the heat balance and refined integral methods to determine this exponent as part of the solution process, allowing the exponent to be time-dependent. From comparing the approximate solutions with numerical and exact analytical solutions whenever possible, we show that the CIM greatly improves the accuracy on standard heat balance integral methods, without detracting from its simplicity.

1. Introduction

Phase-change, or Stefan, problems in which a material melts or solidifies occur in a wide variety of natural and industrial processes. Mathematically, these are special cases of moving-boundary problems, where the location of the front between the liquid and solid is not known a priori, but must be determined as part of the solution. In the classical one-dimensional Stefan problem, which is most studied in the literature, the phase change occurs due to a constant heating or cooling temperature. However, it is more practically relevant to consider the situation where a heat flux or convective boundary condition is imposed.

In this paper we apply a combination of conventional heat balance and refined integral methods (HBIMs and RIMs, respectively) to the two-phase Stefan problem where the second phase first appears only after a finite delay time. The analysis is based on a solidification problem but it could easily be recast as a melting problem. Our aim is to develop an integral method that provides a more accurate description of the process. The main advantage of these integral methods is that they significantly reduce the complexity of the problem. In the first stage of the process, called the pre-solidification stage, there is only a liquid region and thus no moving boundary. For both a heat-flux and Robin boundary condition we can write down an exact solution; this can then be compared with the CIM solution. The method involves introducing a heat penetration depth $\delta(t)$, whereby for $x > \delta$ the temperature change above the initial temperature is assumed to be negligible. Then an approximating function is defined for the temperature, typically a polynomial, and by applying sufficient boundary conditions at $x = 0$ and $x = \delta$, all the unknown coefficients can be determined in terms of the unknown function δ. Finally, the governing heat equation is integrated for $x \in [0, \delta]$ to produce a heat balance integral, leading to an ordinary differential

E-mail address: sarah.mitchell@ul.ie.

http://dx.doi.org/10.1016/j.cam.2014.11.051
0377-0427/

equation to solve for δ [1,2]. This stage ends when the temperature at $x = 0$ has reduced to the solidification temperature. The second stage of the process, which consists of both the liquid and solid phases, is governed by two heat equations coupled to a Stefan condition. In this stage we specify polynomial profiles in both the liquid and solid regions, and this allows us to determine the location of the solidification front as it moves with time.

Goodman [3] originally proposed the *heat balance integral method* (HBIM) for solving thermal and Stefan problems, which was an adaptation of the Karman–Pohlhausen integral method [4] for analysing boundary layers; see [5] for a translated account of this work. Since exact solutions have been found for many problems in heat transfer, the HBIM has made its greatest impact on Stefan problems, where very few exact solutions exist. Their popularity arises from their simplicity and the fact that they produce analytic solutions for a wide range of problems and parameter values. However, it should be noted that they are not always as accurate as numerical solutions. In the last few years Mitchell and Myers [6–9,2,10–14] have published a series of papers devoted to integral methods applied to a variety of thermal and moving boundary problems. A comprehensive review of the HBIM and its variants is given in [9], along with a discussion of its disadvantages. Mitchell and Myers have also investigated ways to improve the HBIM by using an unknown exponent in the approximating profile to describe the dependent variable (usually the temperature) [2,11–13], and these have always given more accurate solutions than the classic HBIM solutions. The CIM solution combines the HBIM and RIM solutions and allows the exponent of the approximating function to be time-dependent [2,13]. Myers [11,12] has employed an alternative method to determine the exponent by minimising an error function. Whilst this can sometimes improve on the CIM in certain cases, it does not easily allow for situations when the exponent is time-dependent and the minimisation can be complicated. In addition, it is not clear how to apply the Myers method in situations with two-stages, or even three-stages if the domain is finite. This is discussed in more detail in Section 4.

A recent paper by Mitchell [1] applies the CIM to the two-stage, one-phase, ablation problem, which is defined as the removal of a material from the surface of an object by vaporisation, chipping or other erosive processes. The CIM gives dramatically improved results to standard HBIM methods, by showing that the exponent in the approximating function was time-dependent, and that using a constant value was very inaccurate. This improvement motivated considering an application with two phases which also had a delay in the onset of phase change. This has only previously been studied numerically by Mitchell and Vynnycky [15], and this was in the restricted case where the domain of the liquid region was always assumed to be semi-infinite. Whilst we also treat this case in detail here, we also consider finite domains, which are far more realistic but more complicated to analyse.

The layout of this paper is as follows. In Section 2 we formulate the governing non-dimensional equations to describe the two-phase Stefan problem with the delayed onset of phase change, using a heat-flux boundary condition. In Section 3 we apply the CIM to the problem on a semi-infinite domain and discuss the Robin boundary condition, motivating how the boundary condition could arise from including how to model the surface that the liquid region rests upon. Section 4 extends the analysis to the case where the domain of the liquid is finite, and discusses the different cases that arise depending on the size of the domain. All the integral method solutions are compared with a numerical solution, the details of which are given in the Appendix. Finally, in Section 5 we draw conclusions.

2. Mathematical formulation

Consider the cooling of a liquid, occupying the half-plane $y > 0$, that is initially at a temperature, T_{hot}, which is greater than its melting temperature, T_{melt}, and which is cooled at $y = 0$ for time $t > 0$ by an applied heat flux $Q(t)$. After cooling commences, the temperature of the liquid decreases until some time t_m, at which stage solid begins to form at $y = 0$; subsequently, solid occupies the region $0 \le y \le y_m(t)$ and liquid occupies $y > y_m(t)$, where $y_m(t)$ denotes the location of the solidification front. A schematic is shown in Fig. 1.

Assuming the material properties of the solid and liquid phases to be constant, the governing equations are as follows. For $0 < t < t_m$ and $y > 0$, and then $t > t_m$ and $y > y_m(t)$ we have

$$\rho_l c_{pl} \frac{\partial T_l}{\partial t} = k_l \frac{\partial^2 T_l}{\partial y^2}, \tag{1}$$

where T_l is the liquid temperature, k_l is the thermal conductivity of the liquid, c_{pl} is its specific heat capacity and ρ_l its density. For $t > t_m$ and $0 < y < y_m(t)$, we have

$$\rho_s c_{ps} \frac{\partial T_s}{\partial t} = k_s \frac{\partial^2 T_s}{\partial y^2}, \tag{2}$$

where T_s is the solid temperature, k_s is the thermal conductivity of the solid, c_{ps} is its specific heat capacity and ρ_s its density. We assume henceforth that $\rho_l = \rho_s = \rho$.

For boundary conditions, we have, at $y = y_m(t)$,

$$T_s = T_l = T_{melt}, \tag{3}$$

and the Stefan condition,

$$k_s \frac{\partial T_s}{\partial y} - k_l \frac{\partial T_l}{\partial y} = \rho \Delta H_f \frac{dy_m}{dt}, \tag{4}$$

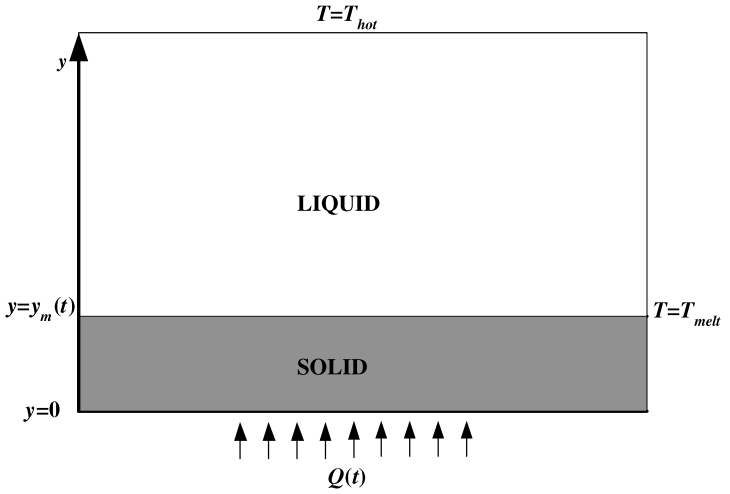

Fig. 1. System geometry.

where ΔH_f is the latent heat of fusion. At $y = 0$, we have

$$\begin{cases} k_l \dfrac{\partial T_l}{\partial y} = Q(t) & \text{for } 0 \le t \le t_m, \\ k_s \dfrac{\partial T_s}{\partial y} = Q(t) & \text{for } t_m < t, \end{cases} \tag{5}$$

where $Q(t) > 0$. Also, as $y \to \infty$ we have

$$T_l \to T_{hot}. \tag{6}$$

For finite domains, say $y_m(t) < y < Y$, then this condition is replaced by

$$\frac{\partial T_l}{\partial y} = 0 \quad \text{at } y = Y. \tag{7}$$

We assume that $Q(t) \equiv Q$ is constant henceforth, in order to allow analytical progress in the pre-solidification stage $0 < t < t_m$.

Since governing equations (1) and (2) are both parabolic PDEs, initial conditions for T_l and T_s are necessary at $t = 0$ and $t = t_m$, respectively. For T_l, we take

$$T_l = T_{hot} \quad \text{at } t = 0, \tag{8}$$

whereas for T_s it follows that

$$T_s = T_{melt} \quad \text{at } t = t_m. \tag{9}$$

In addition, we must have

$$y_m(t_m) = 0. \tag{10}$$

It is more convenient to proceed in nondimensional variables. To do this, we write

$$y' = \frac{y}{[y]}, \qquad y'_m = \frac{y_m}{[y]}, \qquad t' = \frac{t}{[t]}, \qquad T'_{l,s} = \frac{T_{melt} - T_{l,s}}{\Delta T}, \tag{11}$$

where $\Delta T = T_{hot} - T_{melt}$, and $[y]$ and $[t]$ are length and time scales, respectively; the latter two are to be determined. We choose these from the pre-solidification phase by taking $[t]$ from the heat equation (1) and $[y]$ from the boundary condition (5); this gives

$$[t] = \frac{\rho c_{pl} [y]^2}{k_l}, \qquad [y] = \frac{k_l \Delta T}{Q}. \tag{12}$$

Eqs. (1) and (2) then become, respectively (after dropping the $(\cdot)'$ notation),

$$\frac{\partial T_l}{\partial t} = \frac{\partial^2 T_l}{\partial y^2} \tag{13}$$

$$\kappa \frac{\partial T_s}{\partial t} = \frac{\partial^2 T_s}{\partial y^2}, \tag{14}$$

where $\kappa = c_{ps}k_l/c_{pl}k_s$. The boundary conditions for T_l and T_s are then

$$T_s = T_l = 0 \quad \text{at } y = y_m(t) \tag{15}$$

$$\beta \frac{\mathrm{d}y_m}{\mathrm{d}t} = \frac{\partial T_l}{\partial y} - K\frac{\partial T_s}{\partial y} \quad \text{at } y = y_m(t) \tag{16}$$

$$\frac{\partial T_l}{\partial y} = -1 \quad \text{at } y = 0, \text{ for } 0 \le t \le t_m \tag{17}$$

$$K\frac{\partial T_s}{\partial y} = -1 \quad \text{at } y = 0, \text{ for } t > t_m \tag{18}$$

$$T_l \to -1 \quad \text{as } y \to \infty, \tag{19}$$

with $K = k_s/k_l$ and $\beta = \Delta H_f/[c_{pl}\Delta T]$ is the inverse Stefan number. The initial conditions (8)–(10) are, respectively,

$$T_l = -1 \quad \text{at } t = 0 \tag{20}$$

$$T_s = 0 \quad \text{at } t = t_m \tag{21}$$

$$y_m(t_m) = 0. \tag{22}$$

Observe that $T_l < 0$ for $0 < t < t_m$ and so t_m is determined as the nondimensional time when $T_l(0, t)$ reaches 0.

3. The semi-infinite domain

We begin by applying the combined heat balance integral method (CIM) to the system above using boundary condition (19). The boundary condition (7), which applies in the finite domain case, is discussed in more detail in Section 4.

3.1. Pre-solidification stage

The exact solution in the pre-solidification stage is then

$$T_l(y, t) = -1 + 2\sqrt{\frac{t}{\pi}}\exp\left(-\frac{y^2}{4t}\right) - y\,\mathrm{erfc}\left(\frac{y}{2\sqrt{t}}\right), \tag{23}$$

and solving $T_l(0, t_m) = 0$ gives $t_m = \pi/4$. The aim is now to apply the CIM to both the pre-solidification and solidification stages, similar to that carried out in [1] for the related one-phase ablation problem. The pre-solidification stage is identical to the pre-ablation stage but for convenience the method is highlighted here.

Firstly, we define the heat penetration depth, $\delta(t)$. For $x \ge \delta$ the temperature change from the initial temperature is negligible and so $T_l(\delta, t) = -1$, $\frac{\partial T_l}{\partial y}(\delta, t) = 0$. Secondly, an approximating function is introduced, typically a polynomial, which is valid over the domain $0 \le y \le \delta(t)$. Thus we choose

$$T_l = -1 + \frac{\delta}{n}\left(1 - \frac{y}{\delta}\right)^n, \tag{24}$$

which satisfies boundary condition (17) and the far field conditions at $y = \delta$, provided that $n > 1$. The CIM involves choosing n as part of the solution process, and this greatly improves the accuracy [2,11–13].

Finally, the heat balance integral is derived from integrating the heat equation over $y \in [0,\ \delta]$. If n is specified then this leads to a single ODE to solve for the unknown δ. The Myers method [11,12] chooses n to minimise the Langford error [16]

$$E_n = \int_0^\delta \left[\frac{\partial T_l}{\partial t} - \frac{\partial^2 T_l}{\partial y^2}\right]^2 \mathrm{d}y, \tag{25}$$

but this forces n to be constant. However, as shown in [1], for phase-change problems involving semi-infinite domains the exponent n is time-dependent. The CIM is less algebraically complex than the Myers method and allows n to vary with time if necessary. It involves combining the HBIM formulation with a RIM (refined integral method) formulation whereby the heat equation is multiplied by y before integrating over $y \in [0,\ \delta]$. We then obtain a pair of ODEs to solve for both δ and n.

The HBIM and RIM formulations are given by

$$\text{HBIM}: \ \frac{\mathrm{d}}{\mathrm{d}t}\int_0^\delta T_l\,\mathrm{d}y + \frac{\mathrm{d}\delta}{\mathrm{d}t} = -\left.\frac{\partial T_l}{\partial y}\right|_{y=0}, \qquad \text{RIM}: \ \frac{\mathrm{d}}{\mathrm{d}t}\int_0^\delta yT_l\,\mathrm{d}y + \delta\frac{\mathrm{d}\delta}{\mathrm{d}t} = -T_l\big|_{y=\delta} + T_l\big|_{y=0}. \tag{26}$$

Substituting T_l from (24) into these integrals leads to the following expressions:

$$\text{HBIM}: \ \frac{\mathrm{d}}{\mathrm{d}t}\left[\frac{\delta^2}{n(n+1)}\right] = 1, \qquad \text{RIM}: \ \frac{\mathrm{d}}{\mathrm{d}t}\left[\frac{\delta^3}{n(n+1)(n+2)}\right] = \frac{\delta}{n}. \tag{27}$$

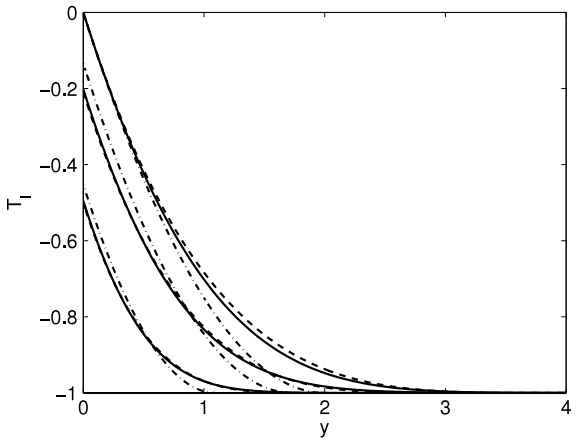

Fig. 2. Pre-solidification stage: Comparison of exact (solid line), CIM (dashed line) and the $n = 2$ HBIM (dot-dashed line) solutions at $t = 0.2$, $t = 0.5$ and $t = t_m$.

As discussed in [1], it turns out that solving both of these equations actually leads to a constant value of n, namely $n = 4$, and then $\delta(t) = \sqrt{n(n+1)t}$. Whilst we could have used the Myers method to give alternative constant values of n (i.e. $n \approx 3.485$ and $n \approx 3.822$ for the HBIM and RIM formulations respectively), the CIM is preferable here to connect to the solidification stage where the exponent is time-dependent. Results in [1] show that both the CIM and Myers Method give very accurate results when compared with the exact solution, and significantly better than the more standard polynomial which uses $n = 2$.

The CIM value of t_m is found from solving $T_l(0, t) = 0$, giving $\delta = n$, which then leads to $t_m = n/(n+1)$. Hence if $n = 4$ it follows that $t_m = 0.8$ which is a 1.859% error. Note that the HBIM solution using $n = 2$ gives $t_m = 2/3$ which is a 15.117% error.

Fig. 2 shows plots of T_l against y at three values of t. We have included the HBIM solution with $n = 2$ for comparison purposes. Observe that the CIM solution is much more accurate.

3.2. Solidification stage

We now consider the solidification stage for $t > t_m$ which has both solid and liquid phases. The polynomial profiles are given by

$$T_s = a\left(1 - \frac{y}{y_m}\right) + \frac{(y_m - Ka)}{mK}\left(1 - \frac{y}{y_m}\right)^m \tag{28}$$

$$T_l = -1 + \left(\frac{\delta - y}{\delta - y_m}\right)^n. \tag{29}$$

These profiles satisfy the boundary conditions (15) and (18). Note that the exponent n is now time dependent but we choose to keep the same labelling for simplification. The initial condition for n is determined from assuming that the profiles (24) and (29) must match at $t = t_m$: since $y_m(t_m) = 0$ this implies that $n(t_m) = 4$.

In profile (28) the coefficient a is unknown, and time-dependent, and must be found using the heat balance integral. The exponent m is also unknown, and can either be specified in advance or determined using the CIM or Myers method. In standard Stefan problems with moving boundary position y_m, this exponent does not tend to vary with time and so a constant value can be used [13]. This motivates using the Myers method to determine m in the solid region.

The HBIM and RIM formulations in the liquid are given by

$$\text{HBIM}: \ \frac{\mathrm{d}}{\mathrm{d}t}\int_{y_m}^{\delta} T_l \,\mathrm{d}y + \frac{\mathrm{d}\delta}{\mathrm{d}t} = -\left.\frac{\partial T_l}{\partial y}\right|_{y=y_m} \tag{30}$$

$$\text{RIM}: \ \frac{\mathrm{d}}{\mathrm{d}t}\int_{y_m}^{\delta} yT_l \,\mathrm{d}y - y_m\frac{\mathrm{d}}{\mathrm{d}t}\int_{y_m}^{\delta} T_l \,\mathrm{d}y + (\delta - y_m)\frac{\mathrm{d}\delta}{\mathrm{d}t} = 1. \tag{31}$$

Note that there is some freedom in the choice of latter integral, as discussed in [1], but this form turns out to be more convenient. Once combined with the HBIM, all RIM formulations lead to the same results.

In the solid, if m is specified with the Myers method then there is a choice of whether to use the HBIM or RIM formulations. In this semi-infinite problem the liquid region dominates over the solid region, at least initially, and choosing the HBIM over

the RIM turns out to make a negligible difference to the results for either y_m or the temperature in the solid. Hence we choose the former as it is simpler to evaluate. The HBIM formulation in the solid is then

$$\kappa \frac{\mathrm{d}}{\mathrm{d}t}\int_0^{y_m} T_s \,\mathrm{d}y = \left.\frac{\partial T_s}{\partial y}\right|_{y=y_m} - \left.\frac{\partial T_s}{\partial y}\right|_{y=0}. \tag{32}$$

Substituting profiles (28) and (29) into the integrals in (30)–(32) leads to the following ODEs:

$$n\frac{\mathrm{d}y_m}{\mathrm{d}t} + \frac{\mathrm{d}\delta}{\mathrm{d}t} - \frac{\delta - y_m}{n+1}\frac{\mathrm{d}n}{\mathrm{d}t} = \frac{n(n+1)}{\delta - y_m} \tag{33}$$

$$n\frac{\mathrm{d}y_m}{\mathrm{d}t} + 2\frac{\mathrm{d}\delta}{\mathrm{d}t} - \frac{(2n+3)(\delta - y_m)}{(n+1)(n+2)}\frac{\mathrm{d}n}{\mathrm{d}t} = \frac{(n+1)(n+2)}{\delta - y_m} \tag{34}$$

$$\left[\frac{(m^2+m-2)a}{2m(m+1)} + \frac{2y_m}{Km(m+1)}\right]\frac{\mathrm{d}y_m}{\mathrm{d}t} + \frac{(m^2+m-2)y_m}{2m(m+1)}\frac{\mathrm{d}a}{\mathrm{d}t} = \frac{1}{\kappa}\left(\frac{1}{K} - \frac{a}{y_m}\right). \tag{35}$$

Finally, the Stefan condition (16) becomes

$$\beta\frac{\mathrm{d}y_m}{\mathrm{d}t} = \frac{Ka}{y_m} - \frac{n}{\delta - y_m}. \tag{36}$$

These four ODEs are used to determine y_m, δ, n and a. The initial conditions are given by $y_m(t_m) = 0$, $\delta(t_m) = n(t_m) = 4$ and $a(t_m) = 0$. The latter condition comes from analysing the governing equations as $t \to t_m^+$, since we know that $y_m \sim \lambda(t - t_m)^{3/2}$ in this limit [10].

An alternative to using profile (28) would be to consider a perturbation expansion in the solid. If we treat κ as a small parameter then T_s can be written as an expansion of the form $T_s = T_{s,0} + \kappa T_{s,1} + \cdots$. The leading order and $\mathcal{O}(\kappa)$ terms satisfy

$$\mathcal{O}(\kappa^0): \ \frac{\partial^2 T_{s,0}}{\partial y^2} = 0, \quad \frac{\partial T_{s,0}}{\partial y}(0,t) = -\frac{1}{K}, \quad T_{s,0}(y_m,t) = 0 \tag{37}$$

$$\mathcal{O}(\kappa^1): \ \frac{\partial^2 T_{s,1}}{\partial y^2} = \frac{\partial T_{s,0}}{\partial t}, \quad \frac{\partial T_{s,1}}{\partial y}(0,t) = 0, \quad T_{s,1}(y_m,t) = 0, \tag{38}$$

which have solutions

$$T_{s,0} = -\frac{1}{K}(y - y_m), \qquad T_{s,1} = \frac{1}{2K}\frac{\mathrm{d}y_m}{\mathrm{d}t}(y^2 - y_m^2), \tag{39}$$

and so the combined expansion is

$$T_s = -\frac{1}{K}(y - y_m) + \frac{\kappa}{2K}\frac{\mathrm{d}y_m}{\mathrm{d}t}(y^2 - y_m^2). \tag{40}$$

The Stefan condition (16) is now

$$\beta\frac{\mathrm{d}y_m}{\mathrm{d}t} = 1 - \kappa y_m\frac{\mathrm{d}y_m}{\mathrm{d}t} - \frac{n}{\delta - y_m}, \tag{41}$$

and so this can be rearranged to give an expression for $\frac{\mathrm{d}y_m}{\mathrm{d}t}$. This is combined with the ODEs (33) and (34) in order to determine y_m, δ and n. An advantage of this method is that we do not have to determine a using (35) but obviously it requires that κ is small in order that the asymptotic expansion is valid.

Typical parameter values corresponding to the continuous casting of copper are given in Table 1 [17]. The non-dimensional variables corresponding to these values are given by $\kappa = 0.4679$, $\beta = 10.3535$ and $K = 2.0938$. Fig. 3 shows the result of y_m against t and T_s and T_l against y. As mentioned above, we use the Myers method to determine m in the solid region. The value obtained is $m = 2.332$, although using $m = 2$ does not noticeably affect the solution. The dot-dashed line in Fig. 3 is the result of using the HBIM in both regions, with m and n found using the Myers method (minimising the Langford errors at $t = t_m$). This leads to values $m = 2.319$ and 3.238. Fig. 4 plots δ and n against t, including their pre-solidification values.

It should be noted that using the asymptotic expansion (40) instead of (28) leads to very similar results, which are indistinguishable on the graphs and so have not been included. This is, in fact, rather surprising given that $\kappa = 0.4679$ but this is probably due to the fact that the solid region is much narrower than the liquid region.

The numerical solution comes from applying the Keller box finite-difference scheme (the details of which are given in the Appendix). The results in Fig. 3 show that the CIM is very accurate for y_m. They are not as good for the temperature profiles but this is probably because β is large. We noticed the same trend with the ablation problem [1], as β increased the results became less accurate. We should also note from Fig. 4 that n does not vary much with time. This is again due to β

Table 1
Parameter values for computations.

Parameter	Value	Unit
c_{pl}	495	J kg^{-1} K^{-1}
c_{ps}	485	J kg^{-1} K^{-1}
k_l	160	W m^{-1} K^{-1}
k_s	335	W m^{-1} K^{-1}
Q	8×10^5	Wm^{-2}
T_{hot}	1,396	K
T_{melt}	1,356	K
T_d	1,300	K
V_{cast}	0.15	m s^{-1}
ρ	8,000	kg m^{-3}
ΔH_f	205,000	J kg^{-1}
Y	0.027	m

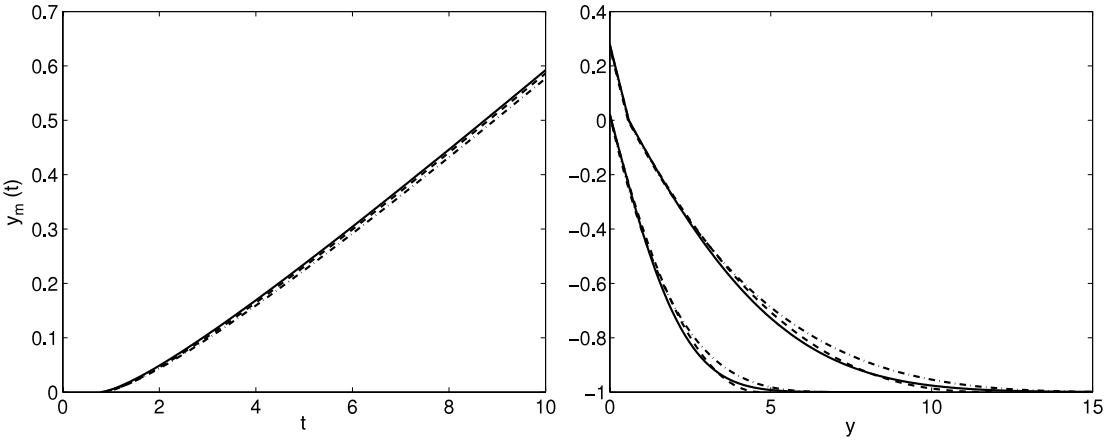

Fig. 3. Comparison of numerical (solid line), CIM (dashed line) and HBIM (dot-dashed line) solutions. Left plot shows y_m against t and right plot shows T_s and T_l against y (at $t = 2$ and $t = 10$).

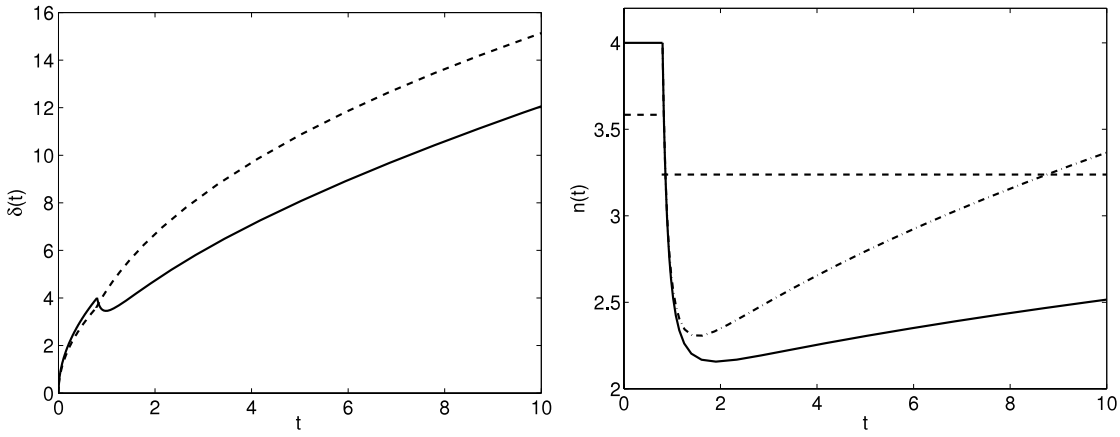

Fig. 4. Left: Plot of δ against t for the CIM (solid line) and HBIM (dashed line) solutions. Right: Plots of n against t. The dot-dashed line shows the n against t for the CIM when $\beta = 4.14$ (rather than $\beta = 10.35$).

being large, if it is reduced then the variation is more pronounced, as shown in Fig. 4; the dot-dashed line is n against t when $\beta = 4.14$ (i.e. $\Delta T = 100$ rather than $\Delta T = 40$). The dip in δ for the CIM was also found in the ablation problem [1]. It can be removed by reducing $n(t_m)$ but then the profiles (24) and (29) will not be consistent at $t = t_m$. Using the HBIM removes the dip, but the results for both y_m and T_l are less accurate, as can be seen in Fig. 3.

3.3. The Robin boundary condition

An alternative to the constant flux boundary condition, which also gives rise to a pre-solidification stage, is to prescribe a Robin boundary condition at $y = 0$. To derive this one could imagine the molten steel resting on a copper surface, in order

to speed up the solidification process. Then we could also model the temperature in the copper via the heat equation

$$\rho c_{pc}\frac{\partial T_c}{\partial t} = k_c\frac{\partial^2 T_c}{\partial y^2}, \tag{42}$$

which holds for $-H < y < 0$, say. The boundary conditions at $y = 0$ are then

$$T_l = T_c \quad \text{and} \quad k_l\frac{\partial T_l}{\partial y} = k_c\frac{\partial T_c}{\partial y}, \tag{43}$$

for $0 \le t \le t_m$, and

$$T_s = T_c \quad \text{and} \quad k_s\frac{\partial T_s}{\partial y} = k_c\frac{\partial T_c}{\partial y}, \tag{44}$$

for $t > t_m$. In addition, we set $T_c = T_d$ at $y = -H$. Using the scalings in (12) we can nondimensionalise (42) to give

$$\frac{c_{pc}k_l}{c_{pl}k_c}\frac{\partial T_c}{\partial t} = \frac{\partial^2 T_c}{\partial y^2}. \tag{45}$$

Now $c_{pc}k_l/[c_{pl}k_c] \ll 1$ and so we can assume a pseudo steady-state equation $\frac{\partial^2 T_c}{\partial y^2} = 0$, returning to the dimensional form, with solution given by

$$T_c = A(y + H) + T_d. \tag{46}$$

Substituting this into either (43) or (44) then leads to a Robin condition at $y = 0$. This is given by

$$k_l\frac{\partial T_l}{\partial y} = \frac{k_c}{H}\left(T_l\big|_{y=0} - T_d\right), \tag{47}$$

for $0 \le t \le t_m$, and

$$k_s\frac{\partial T_s}{\partial y} = \frac{k_c}{H}\left(T_s\big|_{y=0} - T_d\right), \tag{48}$$

for $t > t_m$. In the previous section we chose the spatial scaling $[y]$ from the constant flux condition in the pre-solidification stage. Here we use (47) and therefore set

$$[y] = \frac{Hk_l\Delta T}{k_c(T_{melt} - T_d)}. \tag{49}$$

On nondimensionalising, boundary conditions (47) and (48) become

$$\frac{\partial T_l}{\partial y} = \gamma T_l - 1 \quad \text{at } y = 0, \text{ for } 0 \le t \le t_m \tag{50}$$

$$K\frac{\partial T_s}{\partial y} = \gamma T_s - 1 \quad \text{at } y = 0, \text{ for } t > t_m, \tag{51}$$

where $\gamma = \Delta T/(T_{melt} - T_d)$. Note that setting $\gamma = 0$ leads back to the constant flux case.

3.3.1. Pre-solidification stage

The exact solution in the pre-solidification stage can be found using Laplace transforms. It is given by

$$T_l = -1 + \frac{(\gamma+1)}{\gamma}\operatorname{erfc}\left(\frac{y}{2\sqrt{t}}\right) - \frac{(\gamma+1)}{\gamma}e^{\gamma y+\gamma^2 t}\operatorname{erfc}\left(\frac{y+2\gamma t}{2\sqrt{t}}\right). \tag{52}$$

Setting $T_l(0, t_m) = 0$ leads to the following nonlinear equation to solve for t_m:

$$1 = (\gamma+1)e^{\gamma^2 t_m}\operatorname{erfc}\left(\gamma\sqrt{t_m}\right). \tag{53}$$

Let us now consider applying the HBIM. The profile in (24) is replaced by

$$T_l = -1 + \frac{(\gamma+1)\delta}{n+\gamma\delta}\left(1 - \frac{y}{\delta}\right)^n, \tag{54}$$

which gives (24) when $\gamma = 0$, as expected. Using the HBIM and RIM integrals in (26), and substituting in the profile T_l, leads to expressions

$$\text{HBIM}: \ \frac{\mathrm{d}}{\mathrm{d}t}\left[\frac{\delta^2}{(n+\gamma\delta)(n+1)}\right] = \frac{n}{n+\gamma\delta}, \qquad \text{RIM}: \ \frac{\mathrm{d}}{\mathrm{d}t}\left[\frac{\delta^3}{(n+\gamma\delta)(n+1)(n+2)}\right] = \frac{\delta}{n+\gamma\delta}. \tag{55}$$

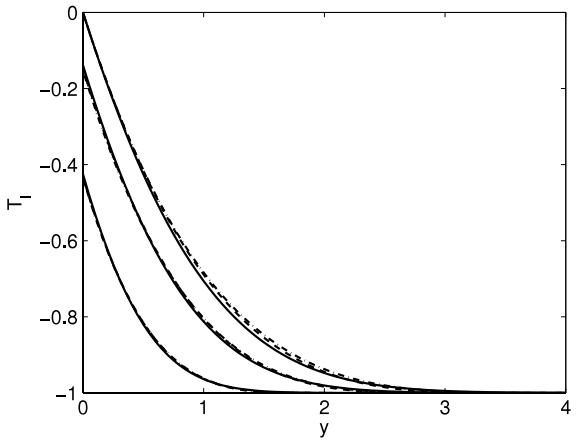

Fig. 5. Pre-solidification stage: comparison of exact (solid line), CIM (dashed line) and the $n = 4$ HBIM (dot-dashed line) solutions at $t = 0.2$, $t = 0.5$ and $t = t_m$.

As discussed in [2], the exponent n is time-dependent for this boundary condition and so the resulting ODEs in (55) must be solved numerically to determine δ and n. The initial condition for n comes from the constant flux case: since $T_l(y, 0) = -1$ it follows that (50) becomes $\frac{\partial T_l}{\partial y} = -(\gamma + 1)$ at $t = 0$ and then we can refer to the CIM value of n found in Section 3.1, namely $n(0) = 4$. Note the factor $\gamma + 1$ drops out of the HBIM and RIM formulations in (26) and so the boundary condition $\frac{\partial T_l}{\partial y} = -(\gamma + 1)$ at $y = 0$ gives the same CIM value for n as the boundary condition $\frac{\partial T_l}{\partial y} = -1$.

We set $T_d = 1300$ K which means that $\gamma = 0.714$. Then the value of t_m found from solving (53) is given by $t_m \approx 0.628008$. The CIM value is $t_m \approx 0.645072$ which is a 2.72% error and the HBIM value (with $n = 4$) is $t_m \approx 0.674871$, giving a 7.46% error. Fig. 5 shows the CIM solution compared with the exact solution. We have not plotted the HBIM solution with $n = 2$ as this is again very inaccurate. We can see that the CIM gives more accurate results than using a constant value of n (the time-dependent CIM exponent is plotted in Fig. 7).

3.3.2. Solidification stage

In the solidification stage, $t > t_m$, the profile for T_l is given by (29); instead of (28), the profile for T_s which satisfies (51) is

$$T_s = a\left(1 - \frac{y}{y_m}\right) + \frac{[y_m - (K + \gamma y_m)]}{mK + \gamma y_m}\left(1 - \frac{y}{y_m}\right)^m. \tag{56}$$

The initial condition for n comes from noting that the profiles T_l in (54) and (29) must match at $t = t_m$. This implies that $(1 + \gamma)\delta = n + \gamma\delta$ which reduces to $\delta = n$. Thus $n = \delta(t_m)$ gives the initial condition for the exponent in the liquid.

Results are given in Figs. 6 and 7. We have not included the HBIM solution with m and n found from minimising the Langford error; again this leads to less accurate results than with the CIM. Comparing Figs. 3 and 6 we see that there is surprisingly little difference between the constant flux and Robin boundary conditions. Increasing γ does lead to a larger variation, as expected.

4. The finite domain

In practice, the domain of the liquid region will be finite. We now consider this more realistic situation and assume that the dimensional domain in the liquid is $y_m < y < Y$, where Y is fixed. Then the boundary condition (6) is replaced by

$$\frac{\partial T_l}{\partial y} = 0, \quad \text{at } y = Y. \tag{57}$$

We only consider the constant flux boundary condition as the analysis for the Robin condition is similar. Using the same scalings as in (12) we re-write the dimensional domain $0 < y < Y$ as $0 < y' < Y/[y]$, or, after dropping the primes this becomes $0 < y < h$ where $h = Y/[y]$. Then the non-dimensional version of (57) is

$$\frac{\partial T_l}{\partial y} = 0, \quad \text{at } y = h. \tag{58}$$

Note that we could re-scale y with Y, however we find it more convenient to keep the scalings as close to the semi-infinite case as possible, to allow easier comparison with the previous analysis. Using parameter values from Table 1 we find that the non-dimensional value is $h = 3.375$ which is still $\mathcal{O}(1)$ and so the above scaling is reasonable.

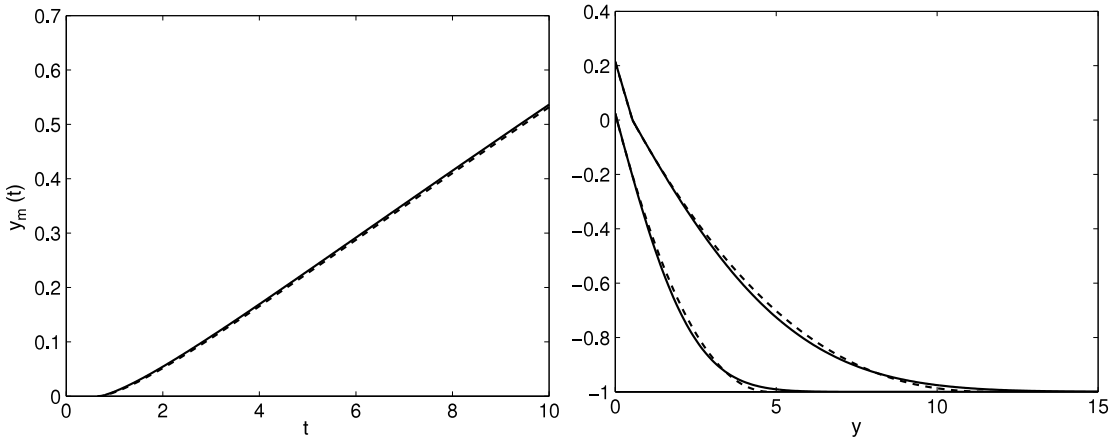

Fig. 6. Comparison of numerical (solid line) and CIM (dashed line) solutions for the Robin boundary condition. Left plot shows y_m against t and right plot shows T_s and T_l against y (at $t = 2$ and $t = 10$).

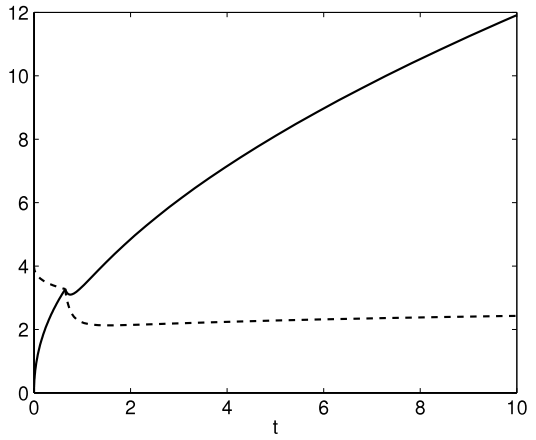

Fig. 7. Plot of δ (solid line) and n (dashed line) against t for the CIM (Robin boundary condition).

The exact solution in the pre-solidification stage can be found using either separation of variables or Laplace transforms. The latter turns out to be more convenient (for comparison with the semi-infinite case) and we find

$$T_l(y,t) = -1 + \sum_{k=0}^{\infty}\left[2\sqrt{\frac{t}{\pi}}\exp\left(-\frac{[2h(k+1)-y]^2}{4t}\right) - [2h(k+1)-y]\operatorname{erfc}\left(\frac{2h(k+1)-y}{2\sqrt{t}}\right)\right] + \sum_{k=0}^{\infty}\left[2\sqrt{\frac{t}{\pi}}\exp\left(-\frac{[2hk+y]^2}{4t}\right) - [2hk+y]\operatorname{erfc}\left(\frac{2hk+y}{2\sqrt{t}}\right)\right], \tag{59}$$

and so the exact value of t_m is found from solving the nonlinear equation $T_l(0, t_m) = 0$, which reduces to

$$1 = 2\sqrt{\frac{t_m}{\pi}} + 2\sum_{k=1}^{\infty}\left[2\sqrt{\frac{t_m}{\pi}}\exp\left(-\frac{h^2k^2}{t_m}\right) - 2hk\operatorname{erfc}\left(\frac{hk}{\sqrt{t_m}}\right)\right]. \tag{60}$$

Note that the second term is small and so $t_m \approx \pi/4$ (when $h = 3,\ 4,\ 5$, $|t_m - \pi/4| = 1.29 \times 10^{-6},\ 1.02 \times 10^{-10},\ 6.66 \times 10^{-16}$ respectively).

In the pre-solidification stage it makes sense to initially use the profile (24). Although it assumes that the condition $T_l(\delta, t) = -1$ holds, this is reasonable and will be valid for small times. This follows the work in Myers et al. [14], which considered applying the heat balance integral method to the melting of a finite block of ice. The condition $T_l(\delta, t) = -1$ will no longer be valid when δ reaches h, which gives a way to quantify when the temperature at $y = h$ starts to increase. The CIM predicted value of the end of this stage is $t_m = n/(n+1) = 0.8$ when $n = 4$, and this in turn leads to $\delta(t_m) = n = 4$. It is therefore clear that the size of h compared to this value is crucial. If $h < \delta(t_m)$ then δ will reach the right boundary before

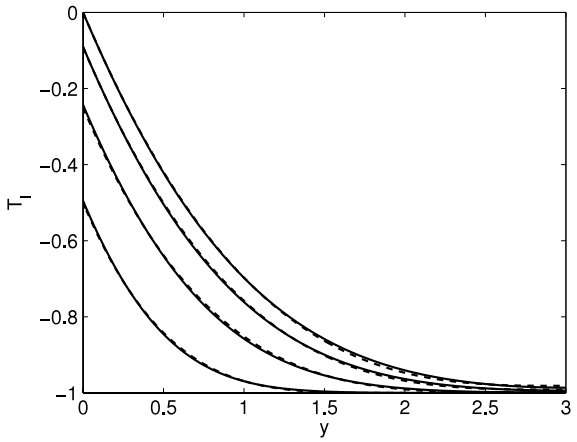

Fig. 8. The case $h \leq \delta(t_m)$: Plot of T_l against y in the pre-casting stage at times $t = 0.2,\ 0.45,\ 0.65,\ t_m$, with $h = 3$. The solid line denotes the exact solution (59) and the dashed line denotes either (24) or (61), depending on the size of t compared with t_h.

the solidification stage begins, say at time t_h. We will therefore have to switch to an alternative profile not involving δ for the time period $t \in [t_h,\ t_m]$.

If $h > \delta(t_m)$ then we can use profile (24) throughout the whole pre-solidification stage. The switch in profile to one not containing δ will then arise in the solidification stage. Recall that the parameter values in Table 1 give $h = 3.375 < \delta(t_m)$. However, for generality we will describe the cases $h \leq \delta(t_m)$ and $h > \delta(t_m)$ separately.

4.1. The case $h < \delta(t_m)$

The expression for δ in the pre-solidification stage is given by $\delta = \sqrt{n(n+1)t}$. Thus δ reaches h at time $t_h = h^2/[n(n+1)]$ and we must specify an alternative profile for $t \in [t_h,\ t_m]$. We then follow [14] and introduce the unknown quantity $T_l(h, t) = f(t)$ which has initial condition $f(t_h) = -1$. The corresponding profile that satisfies this condition and boundary conditions (17) and (58) is given by

$$T_l = f(t) + \frac{h}{n}\left(1 - \frac{y}{h}\right)^n. \tag{61}$$

We will assume that n is time-dependent and then its initial condition comes from the fact that the profiles (24) and (61) must match at $t = t_h$, i.e. $n(t_h) = 4$. Applying the HBIM and RIM formulations, but now integrating over $y \in [0,\ h]$, leads to the following pair of ODEs to solve for f and n:

$$h\frac{\mathrm{d}f}{\mathrm{d}t} - \frac{(2n+1)h^2}{n^2(n+1)^2}\frac{\mathrm{d}n}{\mathrm{d}t} = 1 \tag{62}$$

$$\frac{h}{2}\frac{\mathrm{d}f}{\mathrm{d}t} - \frac{(3n^2+6n+2)h^2}{n^2(n+1)^2(n+2)^2}\frac{\mathrm{d}n}{\mathrm{d}t} = \frac{1}{n}. \tag{63}$$

Although we could eliminate $f'(t)$ and integrate to obtain an implicit expression for $n(t)$, this solution does not allow us to analytically determine f or t_m (which is the time when $f(t_m) + h/n(t_m) = 0$, as seen from setting $T_l(0, t_m) = 0$ in (61)). Thus we numerically solve (62) and (63) and iterate on t to find t_m, only stopping when the condition $f(t_m) + h/n(t_m) < 0$ is violated.

In Fig. 8 we plot T_l against y in the pre-casting stage when $h = 3$. Then $t_h = 0.45$ and so the profile (24) is valid for $0 < t \leq 0.45$ and the profile (61) is valid for $0.45 < t < t_m$. The absolute error between the exact and CIM predicted values of t_m is 3.61×10^{-3}. Fig. 8 shows that the CIM profile gives a very accurate approximation of the exact solution, and that the temperature at $y = h$ starts to rise for $t > t_h$, as expected.

In the solidification stage the profile for T_s is again given by (28) and we choose a polynomial profile similar to (29) but incorporating $f(t)$, and with δ replaced by h, i.e.

$$T_l = f(t)\left[1 - \left(\frac{h-y}{h-y_m}\right)^n\right]. \tag{64}$$

The initial conditions for f and n are the values from the pre-solidification stage at $t = t_m$.

Similar to those given in (30), the HBIM and RIM formulations in the liquid are given by

$$\text{HBIM}: \ \frac{\mathrm{d}}{\mathrm{d}t}\int_{y_m}^{h} T_l\,\mathrm{d}y = -\left.\frac{\partial T_l}{\partial y}\right|_{y=y_m}, \qquad \text{RIM}: \ \frac{\mathrm{d}}{\mathrm{d}t}\int_{y_m}^{h} yT_l\,\mathrm{d}y - y_m\frac{\mathrm{d}}{\mathrm{d}t}\int_{y_m}^{h} T_l\,\mathrm{d}y = -f(t). \tag{65}$$

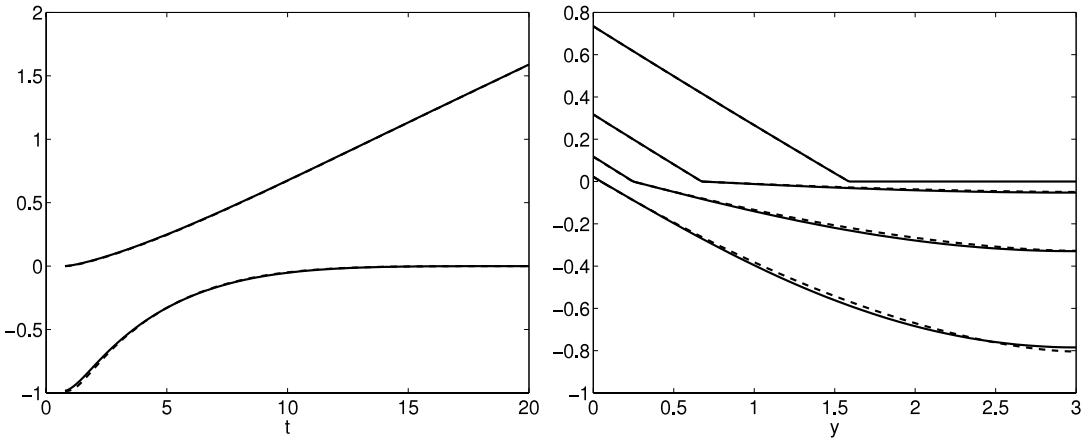

Fig. 9. The case $h < \delta(t_m)$: comparison of numerical (solid line) and CIM (dashed line) solutions in the solidification stage, with $h = 3$. Left plot shows y_m (upper lines) and f (lower lines) against t and right plot shows T_s and T_l against y (at $t = 2$, $t = 5$, $t = 10$ and $t = 20$).

Substituting profile (64) into these integrals leads to the following ODEs:

$$-n\frac{\mathrm{d}y_m}{\mathrm{d}t} + \frac{n(h-y_m)}{f}\frac{\mathrm{d}f}{\mathrm{d}t} + \frac{h-y_m}{n+1}\frac{\mathrm{d}n}{\mathrm{d}t} = -\frac{n(n+1)}{h-y_m} \tag{66}$$

$$-n\frac{\mathrm{d}y_m}{\mathrm{d}t} + \frac{n(n+3)(h-y_m)}{2f}\frac{\mathrm{d}f}{\mathrm{d}t} + \frac{(2n+3)(h-y_m)}{(n+1)(n+2)}\frac{\mathrm{d}n}{\mathrm{d}t} = -\frac{(n+1)(n+2)}{h-y_m}. \tag{67}$$

The ODE in the solid is again given by (35) and the Stefan condition (16) becomes

$$\beta\frac{\mathrm{d}y_m}{\mathrm{d}t} = \frac{Ka}{y_m} + \frac{nf}{h-y_m}. \tag{68}$$

Note that if $h = 4$, i.e. $h = \delta(t_m)$, then the same ODEs hold but now the initial conditions in the liquid are $f(t_m) = -1$ and $n(t_m) = 4$.

Figs. 9 and 10 show results in the solidification stage, again with $h = 3$, and we can see that the profiles for y_m and f are very accurate. The height function f tends to zero fairly quickly, which then means that the liquid temperature has reached zero. These plots have been generated by including T_l right up until the time when y_m reaches h, but we could simply solve for the equations in the solid once f reaches zero. However, we would then have to estimate the time taken for f to reach zero, and this would not be easy as f appears to decay exponentially. The results for T_s and T_l are fairly good though not as accurate as for y_m. Fig. 10 shows n against t throughout the whole process, along with δ against t in the pre-solidification stage. Observe that n quickly decays to a constant value, and this is well before f has reached zero. Despite this, the CIM gives a consistent way to choose n, and is therefore preferable to applying the HBIM and trying to determine this using the Myers method. In fact, if we consider applying the HBIM to T_l in the pre-solidification stage then the ODE in (62) reduces to $f'(t) = 1/h$, which has solution

$$f(t) = \frac{1}{h}(t - t_h) - 1.$$

Apart from the fact that Fig. 9 shows that f is not linear near $t = t_h$, the Langford error (25), but with δ replaced by h, becomes

$$E_n = \frac{2(n^2 - 3n + 1)}{h(n-1)(n-2)},$$

and this does not have a minimum.

4.2. The case $h > \delta(t_m)$

Since $\delta(t_m)$ is less than h, the pre-solidification stage is identical to that in Section 3.1 for the semi-infinite domain. The solidification stage is now separated into two parts, the first whilst $\delta < h$, corresponding to time $t < t_h$ where $\delta(t_h) = h$, and then the second where $f(t)$ is introduced, with $f(t_h) = -1$ and the profile in the liquid given by (64).

Figs. 11 and 12 show analogous results to those in Figs. 9 and 10, but now with $h > \delta(t_m)$. Again the results are very accurate, with those for y_m and f being slightly better than those for the temperatures. In Fig. 11 we see that the front moves a bit slower and f takes longer to reach 0; this is to be expected since the domain is larger. The exponent n, as displayed in Fig. 12, again quickly decays to a constant value and there is now a pronounced dip in δ, also observed in the results for the finite domain (see Figs. 4 and 7) although to a lesser extent.

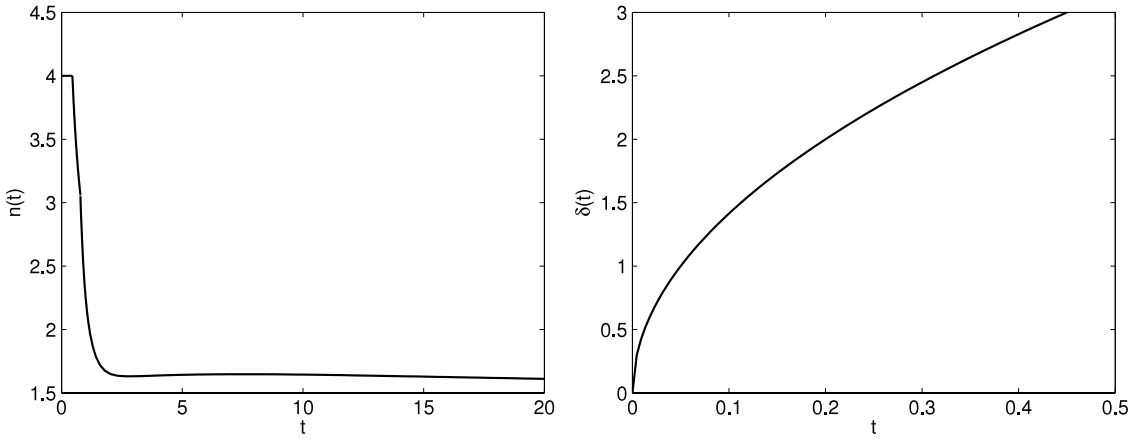

Fig. 10. The case $h < \delta(t_m)$: Plot of n against t (left) and δ against t (right) for the CIM.

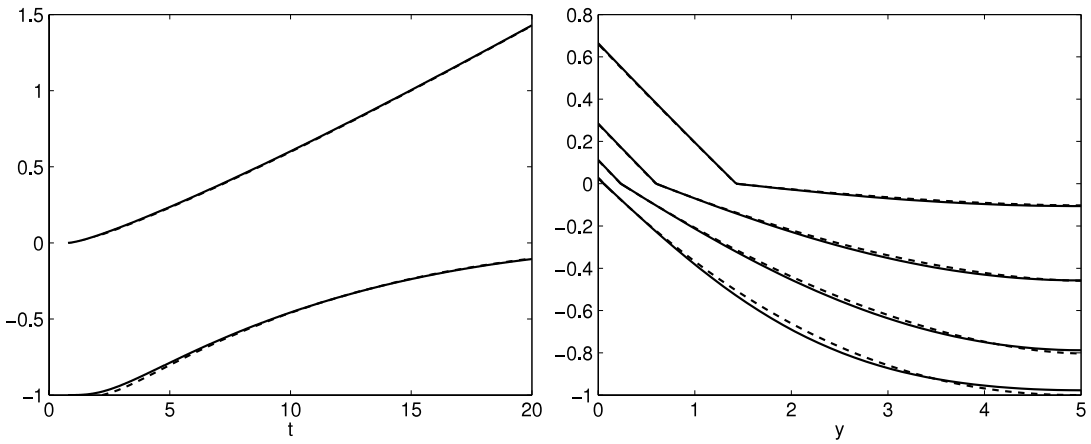

Fig. 11. The case $h > \delta(t_m)$: Comparison of numerical (solid line) and CIM (dashed line) solutions in the solidification stage, with $h = 5$. Left plot shows y_m (upper lines) and f (lower lines) against t and right plot shows T_s and T_l against y (at $t = 2$, $t = 5$, $t = 10$ and $t = 20$).

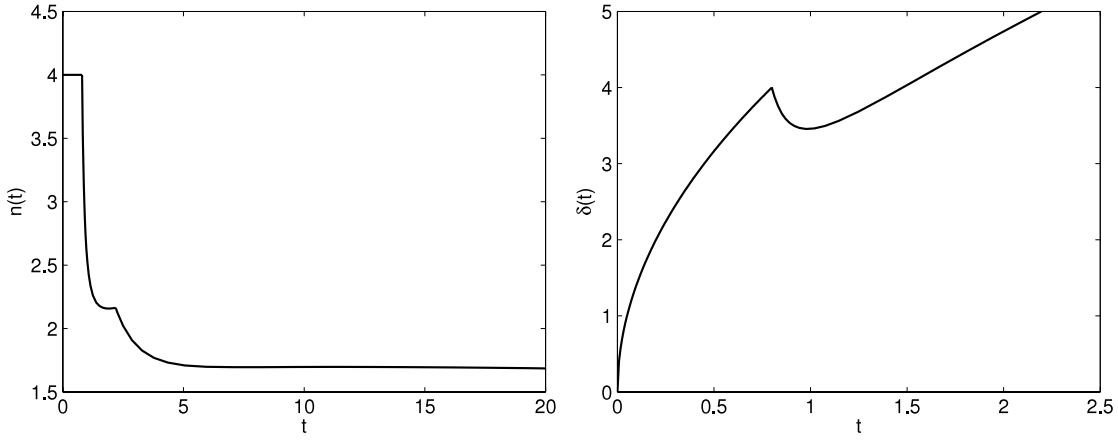

Fig. 12. The case $h > \delta(t_m)$: Plot of n against t (left) and δ against t (right) for the CIM.

5. Conclusions

In this study we have applied the CIM to a non-standard two-phase Stefan problem with delayed onset of phase change. The inclusion of a pre-solidification stage complicates the analysis, especially since the exponent of the approximating function describing the liquid temperature needs to be chosen carefully to match with the profile in the solidification

stage. The size of this exponent is key to providing an accurate solution. Unlike the ablation problem considered in [1], the exponent n does not show much variation in time. However, the CIM does give a consistent way to determine n and ensures that the profiles in both stages are consistent as $t \to t_m$. Whilst the results for the temperature in the liquid are not as accurate as for the ablation problem, we have concentrated on a particular set of parameter values and decreasing β does give improvement (and more variation in n with t). Also, the results for the location of the solidification front y_m are very accurate, and estimating this value carefully is more useful than the temperatures. In fact, a vast majority of the literature on Stefan problems only shows results for the moving boundary position.

In addition, a further complication arises from forcing the domain of the liquid to be finite, and this leads to extra stages depending on the size of δ and the non-dimensional domain size h. The heat penetration depth δ now only features in the model for a shorter period of time, after which the CIM gives very accurate results when compared to the numerical solution.

Finally, it should be noted that the CIM removes the choice between whether to use the HBIM or RIM formulations, both of which can be shown to be the most accurate in certain situations and for certain parameter values [9]. This ambiguity is one reason why these integral methods have been criticised. The method presented here uses both formulations and simply gives an extra term in the resulting ODEs, which involves the first derivative of the exponent n. Although the CIM is more complicated than the standard HBIM, it does give much more accurate results and involves nothing more than solving an extra ODE. Also, the CIM is much simpler than solving the problem numerically, such as that described in the Appendix, since then boundary immobilisations must be applied to transform the domains and the situation becomes even more problematic when solving numerically in both stages [15].

Acknowledgement

The author acknowledges the support of MACSI, the Mathematics Applications Consortium for Science and Industry (www.macsi.ul.ie), funded by the Science Foundation Ireland Investigator Award 12/IA/1683.

Appendix. Numerical solution for $t > t_m$

Returning to the relevant equations in (13)–(23) for $t > t_m$, we change variables by setting

$$\xi = \frac{y}{y_m}, \quad \text{for } y < y_m, \quad \text{and} \quad \eta = y - y_m, \quad \text{for } y \geq y_m, \tag{69}$$

with

$$T_s(y,t) = y_m F(\xi, t), \quad 0 \leq \xi < 1, \tag{70}$$

$$T_l(y,t) = G(\eta, t), \quad 0 \leq \eta < \infty. \tag{71}$$

Then, we solve (denoting $\dot{y}_m = \frac{\mathrm{d}y_m}{\mathrm{d}t}$ for convenience)

$$\frac{\partial^2 F}{\partial \xi^2} = \kappa \left(y_m \dot{y}_m F + y_m^2 \frac{\partial F}{\partial t} - \xi y_m \dot{y}_m \frac{\partial F}{\partial \xi} \right), \quad 0 < \xi < 1 \tag{72}$$

$$\frac{\partial^2 G}{\partial \eta^2} = \frac{\partial G}{\partial t} - \dot{y}_m \frac{\partial G}{\partial \eta}, \quad 0 < \eta < \infty, \tag{73}$$

subject to

$$F = G = 0, \quad \text{at } \xi = 1,\ \eta = 0 \tag{74}$$

$$\beta \dot{y}_m = \frac{\partial G}{\partial \eta} - K \frac{\partial F}{\partial \xi}, \quad \text{at } \xi = 1,\ \eta = 0 \tag{75}$$

$$K \frac{\partial F}{\partial \xi} = -1, \quad \text{at } \xi = 0 \tag{76}$$

$$G \to -1, \quad \text{as } \eta \to \infty \tag{77}$$

$$y_m = 0, \quad \text{at } t = t_m. \tag{78}$$

The initial condition is given by the pre-solidification solution (23), evaluated at $t = t_m$. Thus, on noting that $y = \eta$ at $t = t_m$,

$$G(\eta, t_m) = -1 + 2\sqrt{\frac{t_m}{\pi}} \exp\left(-\frac{\eta^2}{4t_m} \right) - \eta \operatorname{erfc}\left(\frac{\eta}{2\sqrt{t_m}} \right). \tag{79}$$

To determine the initial condition for F, we note that $y_m \sim \lambda (t - t_m)^{3/2}$ as $t \to t_m^+$ [10,15]. In this limit the equations in the solid reduce to

$$F''(\xi) = 0, \qquad F(1) = 0, \qquad KF'(0) = -1, \tag{80}$$

which has solution

$$F(\xi, t_m) = \frac{1}{K}(1-\xi). \tag{81}$$

We can now apply a finite difference scheme to Eqs. (72)–(78), with initial conditions (79) and (81). The Keller box scheme [18–20] is a stable, second-order accurate finite-difference scheme, and is fully implicit since it involves two points at the new time level. It is also very compact since it only uses four neighbouring values in a box formulation.

Following [19] we consider a uniform mesh over the rectangle $t_m \le t \le t_{max}$, $0 \le \xi \le 1$ and $0 \le \eta \le \eta_{max}$, with time step $\Delta t = (t_{max} - t_m)/N$ and spatial steps $\Delta\xi = 1/I$, $\Delta\eta = \eta_{max}/J$ for a given N, I and J. Let W_i^n denote the numerical approximation of a variable W at (x_i, t^n), where x_i is a general spatial discretisation, and define the finite difference operators for the variable W_i^n:

$$\mu_x W_{i+\frac{1}{2}}^{n+\frac{1}{2}} = \frac{1}{2}\left(W_{i+1}^{n+\frac{1}{2}} + W_i^{n+\frac{1}{2}}\right), \qquad \delta_x W_{i+\frac{1}{2}}^{n+\frac{1}{2}} = \frac{1}{\Delta\xi}\left(W_{i+1}^{n+\frac{1}{2}} - W_i^{n+\frac{1}{2}}\right) \tag{82}$$

$$\mu_t W_{i+\frac{1}{2}}^{n+\frac{1}{2}} = \frac{1}{2}\left(W_{i+\frac{1}{2}}^{n+1} + W_{i+\frac{1}{2}}^{n}\right), \qquad \delta_t W_{i+\frac{1}{2}}^{n+\frac{1}{2}} = \frac{1}{\Delta t}\left(W_{i+\frac{1}{2}}^{n+1} - W_{i+\frac{1}{2}}^{n}\right). \tag{83}$$

Then the box scheme consistently uses the operator $\mu_x\delta_t W_{i+1}^{n+\frac{1}{2}}$ to approximate W_t, $\mu_t\delta_x W_{i+1}^{n+\frac{1}{2}}$ to approximate W_x and $\mu_x\mu_t W_{i+1}^{n+\frac{1}{2}}$ to approximate W. It is therefore necessary to re-write the second order Eqs. (72) and (73) as a first order system by setting $U = \frac{\partial F}{\partial \xi}$ and $V = \frac{\partial G}{\partial \eta}$. Then the box scheme applied to (72) is given by

$$\mu_t\delta_\xi F_{i+\frac{1}{2}}^{n+\frac{1}{2}} = \mu_t\mu_\xi U_{i+\frac{1}{2}}^{n+\frac{1}{2}} \tag{84}$$

$$\begin{aligned}\mu_t\delta_\xi U_{i+\frac{1}{2}}^{n+\frac{1}{2}} = \kappa\Bigg[&\left(\mu_t y_m^{n+\frac{1}{2}}\right)\left(\delta_t y_m^{n+\frac{1}{2}}\right)\mu_\xi\mu_t F_{i+\frac{1}{2}}^{n+\frac{1}{2}} + \left(\mu_t y_m^{n+\frac{1}{2}}\right)^2\mu_\xi\delta_t F_{i+\frac{1}{2}}^{n+\frac{1}{2}} \\ &- \left(\mu_\xi\xi_{i+\frac{1}{2}}\right)\left(\mu_t y_m^{n+\frac{1}{2}}\right)\left(\delta_t y_m^{n+\frac{1}{2}}\right)\mu_\xi\mu_t U_{i+\frac{1}{2}}^{n+\frac{1}{2}}\Bigg],\end{aligned} \tag{85}$$

which holds for $i = 0,\ 1,\ \ldots,\ I-1$ and $n = 0,\ 1,\ \ldots,\ N-1$, and the box scheme applied to (73) is given by

$$\mu_t\delta_\eta G_{i+\frac{1}{2}}^{n+\frac{1}{2}} = \mu_t\mu_\eta V_{i+\frac{1}{2}}^{n+\frac{1}{2}} \tag{86}$$

$$\mu_t\delta_\eta V_{i+\frac{1}{2}}^{n+\frac{1}{2}} = \mu_\eta\delta_t G_{i+\frac{1}{2}}^{n+\frac{1}{2}} - \left(\delta_t y_m^{n+\frac{1}{2}}\right)\mu_\eta\mu_t V_{i+\frac{1}{2}}^{n+\frac{1}{2}}, \tag{87}$$

which holds for $i = 0,\ 1,\ \ldots,\ J-1$ and $n = 0,\ 1,\ \ldots,\ N-1$. The boundary conditions in (74), (76) and (77) are $F_I^n = G_0^n = 0$, $KU_0^n = -1$ and $G_J^n = -1$ for $n = 0,\ 1,\ \ldots,\ N$, and the Stefan condition (75) is

$$\beta\left(\delta_t y_m^{n+\frac{1}{2}}\right) = \mu_t V_0^{n+\frac{1}{2}} - K\mu_t U_I^{n+\frac{1}{2}}. \tag{88}$$

Finally, the initial conditions become $y_m^0 = 0$ and

$$F_i^0 = \frac{1}{K}(1-\xi_i), \qquad U_i^0 = -\frac{1}{K}, \quad \text{for } i = 0,\ 1,\ \ldots,\ I \tag{89}$$

$$G_i^0 = -1 + 2\sqrt{\frac{t_m}{\pi}}\exp\left(-\frac{\eta_i^2}{4t_m}\right) - \eta_i\,\mathrm{erfc}\left(\frac{\eta_i}{2\sqrt{t_m}}\right), \qquad V_i^0 = -\mathrm{erfc}\left(\frac{\eta_i}{2\sqrt{t_m}}\right), \quad \text{for } i = 0,\ 1,\ \ldots,\ J. \tag{90}$$

Eqs. (84) and (85) involve y_m^{n+1} and so it is necessary to solve a non-linear equation at each time-step. This is achieved by iterating on y_m, using its value at level n as a starting guess. Then y_m is updated using the Stefan condition (88) until some desired tolerance, ε, is reached. Denoting $y_{m_{(k)}}^{n+1}$ as the values for y_m^{n+1} after k iterations, the convergence criterion used is

$$\left|y_{m_{(k+1)}}^{n+1} - y_{m_{(k)}}^{n+1}\right| < \varepsilon. \tag{91}$$

For the finite domain we use a different transformation to that defined in (69) and (71). Here we set

$$\eta = \frac{y - y_m}{h - y_m}, \qquad T_l(y,t) = (h - y_m)G(\eta, t). \tag{92}$$

Then the liquid region has domain $0 < \eta < 1$ and so η_{max} is replaced by 1 in the discussion above. The right boundary condition (57) then becomes $V_J^n = 0$ for all n and the initial condition in the liquid is given by (59) with y replaced by $h\eta$.

References

[1] S.L. Mitchell, Applying the combined integral method to one-dimensional ablation, Appl. Math. Model. 36 (2012) 127–138.
[2] S.L. Mitchell, T.G. Myers, Improving the accuracy of heat balance integral methods applied to thermal problems with time dependent boundary conditions, Int. J. Heat Mass Transfer 53 (2010) 3540–3551.
[3] T.R. Goodman, The heat-balance integral and its application to problems involving a change of phase, Trans. ASME 80 (1958) 335–342.
[4] K. Pohlhausen, Zur naherungsweisen integration der differentialgleichunger der laminaren grenzschicht, J. Appl. Math. Mech. 1 (1921) 252–290.
[5] H. Schlichting, Boundary Layer Theory, eighth ed., Springer, 2000.
[6] S.L. Mitchell, An accurate nodal heat balance method with spatial subdivision, Numer. Heat Transfer B 60 (2011) 34–56.
[7] S.L. Mitchell, T.G. Myers, Approximate solution methods for one-dimensional solidification from an incoming fluid, Appl. Math. Comput. 202 (1) (2008) 311–326.
[8] S.L. Mitchell, T.G. Myers, A heat balance integral method for one-dimensional finite ablation, AIAA J. Thermophysics 22 (3) (2008) 508–514.
[9] S.L. Mitchell, T.G. Myers, Application of standard and refined heat balance integral methods to one-dimensional Stefan problems, SIAM Rev. 52 (1) (2010) 57–86.
[10] S.L. Mitchell, M. Vynnycky, An accurate finite-difference method for ablation-type Stefan problems, J. Comput. Appl. Math. 236 (2012) 4181–4192.
[11] T.G. Myers, Optimizing the exponent in the heat balance and refined integral methods, Int. Commun. Heat Mass Transfer 36 (2) (2009) 143–147.
[12] T.G. Myers, Optimal exponent heat balance and refined integral methods applied to Stefan problems, Int. J. Heat Mass Transfer 53 (2010) 1119–1127.
[13] T.G. Myers, S.L. Mitchell, An accurate finite-difference method for ablation-type Stefan problems, Appl. Math. Comput. 35 (2011) 4281–4294.
[14] T.G. Myers, S.L. Mitchell, G. Muchatibaya, M.Y. Myers, A cubic heat balance integral method for one-dimensional melting of a finite thickness layer, Int. J. Heat Mass Transfer 5 (2007) 5305–5317.
[15] S.L. Mitchell, M. Vynnycky, On the numerical solution of two-phase Stefan problems with heat-flux boundary conditions, J. Comput. Appl. Math. 264 (2012) 49–64.
[16] D. Langford, The heat balance integral method, Int. J. Heat Mass Transfer 16 (1973) 2424–2428.
[17] M. Vynnycky, A mathematical model for air-gap formation in vertical continuous casting: the effect of superheat, Trans. Indian Inst. Met. 62 (2009) 495–498.
[18] S.L. Mitchell, S.B.G. O'Brien, Asymptotic, numerical and approximate techniques for a free boundary problem arising in the diffusion of glassy polymers, Appl. Math. Comput. 219 (2012) 376–388.
[19] S.L. Mitchell, M. Vynnycky, Finite-difference methods with increased accuracy and correct initialization for one-dimensional Stefan problems, Appl. Math. Comput. 215 (2009) 1609–1621.
[20] S.L. Mitchell, M. Vynnycky, I.G. Gusev, S.S. Sazhin, An accurate numerical solution for the transient heating of an evaporating droplet, Appl. Math. Comput. 217 (2011) 9219–9233.